Journal of Sol-Gel Science and Technology (2024) 110:27–36
https://doi.org/10.1007/s10971-024-06318-8

ORIGINAL PAPER

Facile synthesis of magnetic-fluorescent iron oxide-geothermal silica core/shell nanocomposites via modified sol–gel method

Falah Azizah Elmaria[1,2] · Fauzan Aulia[2] · Luthfiana N. Hidayati[2] · Anis Kristiani[2] · Sudiyarmanto[2] · Yuni Kusumastuti[1] · S. N. Aisyiyah Jenie[2] · Himawan Tri Murti Bayu Petrus[1,3]

Received: 12 October 2023 / Accepted: 17 January 2024 / Published online: 21 February 2024

Abstract

This study successfully synthesizes magnetic fluorescent iron oxide silica core/shell nanocomposites (MFSNC) derived from natural geothermal silica. The nanostructures comprise an iron-oxide core and a fluorescent mesoporous silica outer layer. X-ray diffraction (XRD) analysis indicated diffraction peaks of amorphous silica with crystallites of magnetite types in the MFSNC samples. Transmission electron microscopy combined with energy-disperse X-ray spectroscopy were used to observe the morphological structure, which showed nanoparticles of MFSNC with Fe, Si, O, and N elements. Among varying ratios of ferric salts, the MFSNP0.5 sample exhibited the highest fluorescence intensity (280.5073 a.u.). It demonstrated superior fluorescence stability in water (pH = 7) compared to other samples, as investigated by fluorescence spectrophotometer. Additionally, this sample displayed ferromagnetic properties, with a magnetic saturation (MS) of 14.57 emu/g and a loop area value of 0.7 kOe.emu/g, determined by the vibrating sample magnetometry. This work details the successful synthesis of MFSNC nanocomposites with tailored magnetic and fluorescent properties. Notably, the MFSNC0.5 sample stands out for its superior fluorescence intensity, stability in water, and desirable ferromagnetic characteristics.

Graphical Abstract

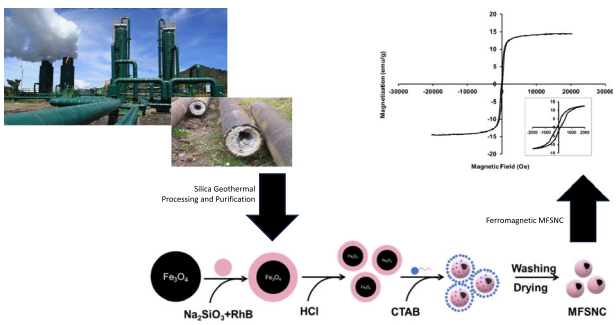

Keywords Magnetic · Silica · Fluorescent · Ferromagnetic · Nanocomposite

✉ Himawan Tri Murti Bayu Petrus
bayupetrus@ugm.ac.id

[1] Department of Chemical Engineering, Faculty of Engineering, Universitas Gadjah Mada, Jalan Grafika No 2, Yogyakarta 55281, Indonesia

[2] Research Center for Chemistry, National Research and Innovation Agency-BRIN, Building 452, Kawasan BJ Habibie, Tangerang Selatan, Banten 15314, Indonesia

[3] Unconventional Geo-Resources Research Center, Faculty of Engineering, Universitas Gadjah Mada UGM, JI, Grafika No. 2, Yogyakarta 55281, Indonesia

Highlights

- Synthesizes magnetic fluorescent iron oxide silica core/shell nanocomposites (MFSNC) derived from natural geothermal silica.
- MFSNC0.5 sample stands out for its superior fluorescence intensity, stability in water, and desirable ferromagnetic characteristics.
- MFSNC displayed ferromagnetic properties, with a magnetic saturation (MS) of 14.57 emu/g and a loop area value of 0.7 kOe.emu/g.

1 Introduction

Magnetic nanoparticles (MNPs) have gained much interest in the material science field due to their wide variety of applications, which includes use as heterogeneous catalysts, absorbents, biosensors, and drug delivery system [1, 2]. These nanoparticles have been reported to be easily functionalized and exhibit superparamagnetic behavior [3]. Iron oxide nanoparticles are a subset of MNPs which are frequently utilized due to their non-toxic nature, affordability, and capacity for easy modification as a result of their unique chemical and physical magnetic characteristics. Hematite (α-Fe_2O_3) is the predominant iron oxide phase, characterized by a hexagonal structure that has ferromagnetic properties. Furthermore, there are two other metastable phases known as maghemite (γ-Fe_2O_3) and magnetite (Fe_3O_4), which exhibit a spinel structure and show ferromagnetic characteristics, respectively [4–7].

Iron oxide nanoparticles can be modified through the addition of other materials, such as organic and inorganic compounds, to produce functional magnetic nano- or microstructures [8, 9]. Iron oxide is frequently coated with an additional outer layer to enhance hydrophilicity and for further surface functionalization [10]. Magnetite (Fe_3O_4) is widely used in nanoparticles synthesis to create magnetic properties in iron oxides. However, it demonstrates an intense tendency to react strongly in the presence of acidic environmental conditions. Therefore, a various materials are utilized as coatings to fabricate the core-shell structure that envelops the magnetite nanoparticles. The materials include silica, carbon, protein, and polymers.

Considering its non-toxic, inert, varying chemical properties, facile surface modification, and high stability, silica oxide has been frequently utilized as an inorganic compound for iron oxide coating [11–13]. The existence of a silica oxide matrix provides 5 between the iron oxide nanoparticles, thoroughly controlling interparticle interactions and preventing agglomeration of the iron oxide nanoparticles. In addition, the silica matrix offers possibilities for surface functionalization with various compounds through employing the silanol groups that exist on the surface [14–17].

Various studies have shown that the magnetic properties and particle size of iron oxides are significantly affected by the methods and treatments developed. The most frequently utilized and convenient method is coprecipitation [18]. Recently, this method has been developed with a wide variety of modification techniques which have no impact on the primary reaction. As a result of combining Fe^{2+} and Fe^{3+} ions, magnetite can be produced and modified to exhibit different sizes and magnetic strengths. A different strategy involves the thermal decomposition of organometallic precursors. Organic iron compounds such as (hydroxylamineferron $[Fe(Cup)_3]$, iron pentacarbonyl $[Fe(CO)_5]$, ferric acetylacetonate $[Fe(acac)_3]$, iron oleate $[Fe(oleate)_3]$ are decomposed at high temperature of the non-polar solvent capping agent. However, it is significant to emphasize that this method is hazardous due to the use of toxic chemicals [19].

The methods used to synthesize magnetic silica nanoparticle core–shell structures have been continuously developed. The microemulsion method is frequently used to produce many different systems that possess both isotropic and thermodynamic stability. Furthermore, the controlling of the atomic ratio of water, oil, and surfactants has contributed to the control of the shape and size distribution of the particles [20]. The Stober process, which utilizes hydrolyzed and condensed TEOS (tetraethyl orthosilicate) in an alcohol-water system with ammonia, is widely recognized as the most popular method. Following a long period of stirring, silica will be synthesized and gradually coated onto the particles' surface by dispersing the original particles in an aqueous alcohol solution, subsequently adding ammonia water and TEOS [21]. Fan et al. reported a study in which they manufactured uniform magnetite using a modified solvothermal approach. They subsequently utilized the Stober process to fabricate monodisperse magnetic silica core-shell nanoparticles [22]. Thermal decomposition that has been defined is also known as an effective method for producing magnetite nanoparticles. The materials were dispersed in cyclohexane with the use of ultrasonic treatment and addition of ammonium hydroxide. Subsequently, TEOS was added, resulting in obtaining of various shell thicknesses for the silica coating [23].

The utilisation of dye-doped silica nanoparticles has been widely studied for various applications including biosensing, bioimaging, forensics, and photocatalysis. These nanoparticles carry unique intrinsic characteristics such as improved photostability and enhanced signal intensity, contributed to a higher concentration of dye molecules per nanoparticle [23, 24]. Since it is unable to absorb visible

light, silica allows the presence of photoactive molecules throughout its matrix, either internally or bound on the surface of the nanoparticles. This structure allows the nanoparticles to exhibit photophysical properties that have similarities with those of the chromophores [20].

The precursors for silica oxide coating might be potentially commonly found (such as TEOS) or derived from nature's products (such as rice husk, bamboo leaves, or geothermal silica) [25]. This study utilizes geothermal silica precipitates as the precursor in order to generate cost-effective, environmentally friendly, and functional nanocomposites using sustainable methods [18]. Geothermal silica precipitate derived from geothermal power plants is known to consist of a large amount of amorphous silica, exceeding 98%, which has the potential to be modified into silica-based nanocomposites [19].

In this study, bifunctional magnetic fluorescent silica core–shell nanocomposites (MFSNC) are synthesized. The outer shell of these nanocomposites is composed of an organic pigment and a geothermal silica-based silica matrix, with iron oxide serving as the core. The geothermal silica-based nanostructures produced by combining magnetic and fluorescent characteristics exhibit the potential to be applied as highly selective biosensing platforms or fluorescent labels.

2 Experimental procedure

2.1 Materials

The silica utilized in this study is derived from the solid residue of the Geodipa Geothermal Power Plant (PLTP). Utilizing this waste is an endeavor towards recycling and repurposing materials which usually appear as byproducts. This research contributes to the development of nanomaterials and supports sustainable practices by utilizing waste from the Geodipa PLTP, thus reducing the environmental impact of industrial waste. Utilizing waste as a raw material may effectively solve sustainability concerns and enhance resource efficiency.

Iron sulfate heptahydrate ($FeSO_4{\cdot}7H_2O$), NaOH, and N-Hydroxysuccinimide (NHS), were purchased from Merck. HCl, rhodamine B, cetyltrimethylammonium bromide (CTAB), undecylenic acid, 1-(3-Dimethylaminopropyl)-3-ethyl carbodiimide (EDC), phosphate-buffered saline (PBS), vancomycin hydrochloride, and sodium broth (NB) were purchased from Sigma-Aldrich. Anhydrous iron (III) chloride ($FeCl_3$) was purchased from Central Drug House (P) Ltd. All chemicals are of analytical grade and used without any further purification. Deionized water sourced from the National Research and Innovation Agency-BRIN was used throughout the whole of work.

2.2 Synthesis of iron oxide

The synthesis of iron oxide, an essential precursor for the MFSNC, was carried out with high accuracy in this precisely conducted experimental approach. A 100 mL solution containing iron (III) chloride ($FeCl_3$) was thoroughly mixed with an equal volume of a solution containing iron sulfate heptahydrate ($FeSO_4{\cdot}7H_2O$). The concentration ratio of the Fe precursors was varied and is shown in Table 1. The systematic mixing of these solutions set the stage for subsequent synthesis processes. Subsequently, 100 mL of sodium hydroxide (NaOH) solution was added dropwise, to attempt to carry out controlled reaction kinetics.

The stepwise addition of sodium hydroxide led to the formation of magnetite (Fe_3O_4), as evidenced by the appearance of a dark solution. The solution obtained was given further processing using a sonication procedure at 65 °C for 30 min. This additional process allowed the production of a black precipitate, identified as magnetite (Fe_3O_4) sample.

Subsequently, the precipitate formed through a filtration process, which was then followed by repeated washing procedures until a neutral pH was achieved. This complete cleansing process effectively eliminated contaminants and unreacted chemicals, contributing to the quality of the final iron oxide product. After the completion of the washing process, the collected precipitate was placed in a controlled drying phase at a temperature range of 80 °C for 5 h. The application of this controlled drying procedure led to the formation of a dry powder, indicating the isolation of iron oxide nanoparticles.

2.3 Synthesis of magnetic fluorescent silica nanocomposites (MFSNC)

In this procedure, 10 g of SiO_2 was accurately weighed and dissolved in 400 mL of 1.5 N NaOH. The mixture was stirred for 1 h at 90 °C, and then the Na_2SiO_3 solution was separated from the impurities through filtration. Subsequently, 5 g of magnetite (Fe_3O_4) and 2.5 mg/g of rhodamine B were added into the sodium silicate solution and

Table 1 Concentration of Fe^{2+} and Fe^{3+} for each MFSNC sample

Sample ID	Concentration	
	$FeCl_3$	$FeSO_4{\cdot}7H_2O$
MFSNC0.5	0.5 M	1 M
MFSNC1.0	1.0 M	1 M
MFSNC1.5	1.5 M	1 M
MFSNC2.0	2.0 M	1 M

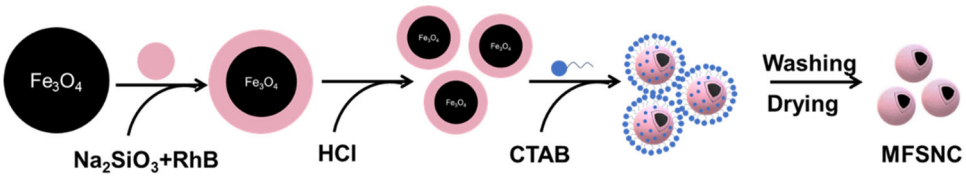

Fig. 1 Schematic of the formation of MFSNC

stirred for 5 min. A 2 N HCl solution was added dropwise until a gel formed at pH 7, which was followed by 2% CTAB was added. The resulting gel was allowed to mature for 18 h at room temperature. After maturation, the gel was washed three times with deionized water until it reached a neutral pH. The sol–gel MFSNC was then dried at 100 °C until it reached a stable weight. The formation of MFSNC is shown in Fig. 1, illustrating the sequential steps involved in the synthesis process. This method provided the effective production and stabilization of mesoporous silica nanocomposites (MFSNC) with the desired properties for advanced applications [18, 19].

2.4 Characterizations

X-ray diffractometry (XRD) was employed to examine the crystalline phases of the magnetic fluorescent silica nanocomposites (MFSNC) and iron oxide. The XRD patterns were recorded on a Rigaku Miniflex 600 diffractometer with Cu Kα-radiation. The data were collected over the 2θ range of 5–90°, with the instrument operated at 45 kV and 40 mA. The investigation of saturation magnetization was performed using a Vibrating Sample Magnetometer manufactured by Dexing Magnet Ltd, which has a measuring capability of 250 Oersted. The optimized MFSNC sample was imaged using a field emission gun-transmission electron microscope (FEG-TEM), Talos F200X (Thermo Fisher Scientific), and an acceleration voltage of 200 kV. The equipment utilized in this study included an Energy Dispersive X-ray (EDX) detector of Super-X type, a High-Angle Annular Dark-Field detector Fishione CL 98 mm, a Scanning Transmission Electron Microscopy Bright-Field and Dark-Field (STEM BF-DF), and a Panther detector with CL 160 mm.

2.5 Fluorescence spectrometer

The solution was prepared by dissolving 10 mg of MFSNC in 10 mL of deionized water, resulting in a sample concentration of 1 mg/mL. The fluorescence intensity of the MFSNC samples was measured using a fluorescence spectrophotometer (Agilent, Singapore) with an excitation wavelength of 545 nm. Emission was observed within the spectral range spanning from 550 to 750 nm. The slit widths of the excitation and emission were both at 5 nm. There was no evidence of filters.

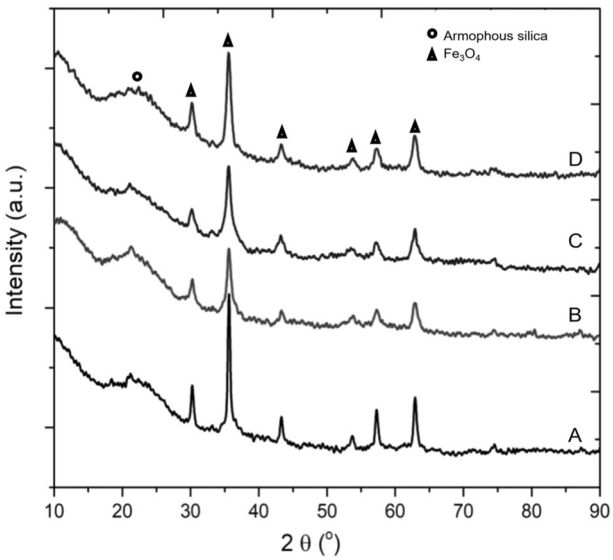

Fig. 2 XRD pattern of MFSNC sample MFSNC0.5 (A), MFSNC1.0 (B), MFSNC1.5 (C), and MFSNC2.0 (D)

3 Result and discussion

The efficient synthesis of magnetite, maghemite, and cobalt ferrite can be achieved by varying certain chemical composition of the nanoparticles and using the iconic molecule separation coprecipitation approach. The synthesis of iron oxide nanoparticles was carried out via the coprecipitation method, which is a facile and effective method to obtain an appropriate yield in a brief amount of time [26]. This method involves the simultaneous precipitation of Fe^{2+} and Fe^{3+} in solution under alkaline conditions (Eq. 1) [27].

$$Fe^{2}{}_{+(aq)} + 2Fe^{3+}_{(aq)} + 8OH^{-}_{(aq)} \rightarrow Fe_3O_{4(s)} + 4H_2O \qquad (1)$$

The iron oxide core was then coated with silica, which was then further functionalized to have an optimum magnetic and fluorescence properties, forming the MFSNC nanocomposites. These bifunctional nanomaterials have been found to be useful as biosensing platforms due to their unique features. The sol–gel method was utilized to synthesize the MFSNC. This method, frequently known as Stober's method, is a conventional approach used for synthesizing nanoparticles. The convenience of this process results from the ease of operation, as well as the fact that it may be carried out at

ambient temperature and pressure, resulting in a higher production yield [28].

Prior to the dispersion of magnetite (Fe_3O_4) in a sodium silicate solution, such solution was prepared through the reaction of SiO_2 and NaOH (Eq. 2). A mixture of sodium silicate, organic dye, and iron oxide undergoes a chemical reaction to produce MFSNC gel. This reaction is catalyzed by hydrochloric acid, as shown by Eq. (3). The organic dye was introduced into silica matrices, while the iron oxide was coated by silica. The final result generated the MFSNC materials [19, 23, 29].

$$SiO_{2(s)} + 2NaOH_{(aq)} \rightarrow Na_2SiO_{3(aq)} \quad (2)$$

$$Na_2SiO_{3(aq)} + Rh\,B_{(aq)} + Fe_3O_{4(s)} + 2HCl_{(aq)} \rightarrow SiO_2 - Fe_3O_4/RhB_{(s)} + 2NaCl_{(aq)} \quad (3)$$

The synthesized MFSNC, with varied Fe^{2+} and Fe^{3+} ratio, were characterized by XRD and the results showed the structure of magnetite for all variations (Fig. 2). The XRD patterns exhibited prominent peaks at 2θ angles of 30.20°; 35.6°; 43.30°; 53.33°; 57.37 and 62.87° corresponding to the (2 2 0), (3 1 1), (4 0 0), (4 2 2), (5 1 1) and (4 4 0) planes of Fe_3O_4 (magnetite), respectively, which are in good agreement with the references values (JCPDS 19–0629) [30–32]. The strong and sharp peaks indicate that all the MFSNC synthesized are crystalline and structurally ordered in a long range. The shape of the iron oxide peak was narrow and sharp, without interference from irregular diffraction peaks, indicating that the iron oxide MFSNC had a higher purity [33].

Figure 2 also showed that the silica peak was shown at an angle of 2θ, precisely between 20° and 30°. Furthermore, the broadening of the peak indicated that the silica of MFSNC is in its amorphous phase. Thus, a certain peak corresponds to the presence of amorphous silica, while other peaks correspond to the presence of crystalline iron oxide. These diffraction peak positions confirmed that the MFSNC nanomaterials containing SiO_2 and Fe_3O_4 had been successfully synthesized [13, 34].

The XRD pattern of MFSNC had a relatively high peak intensity at 2θ, an angle of 35.50° precisely corresponding to the (3 1 1) peak, which indicates the products have an abundance of crystallinity. The average size of the crystallites can be estimated by quantitatively calculating the (3 1 1) peak using the Debye-Scherrer formula (Eq. 4).

$$D = \frac{k \times \lambda}{\beta \times cos\theta} \quad (4)$$

Where λ represents the wavelength of the Cu Kα line, and β is the full width at one-half the maximum (FWHM) of the most intense diffraction peak of the crystallographic plane (3 1 1). In the X-ray diffraction (XRD) analysis, variations in the particle size of the (3 1 1) plane can be observed, and these variations are attributed to the crucial role played by ferric chloride ($FeCl_3$) in the synthesis of iron oxide nanoparticles, specifically magnetite (Fe_3O_4). The concentration of $FeCl_3$ can influence the size of Fe_3O_4 crystallites during the synthesis process as shown in Table 2.

By altering the concentration ratio, particle growth can be controlled during the synthesis process, affecting the final crystallite size. The (3 1 1) plane refers to a specific crystallographic plane in the crystal lattice of Fe_3O_4. The XRD analysis provides insights into the arrangement of atoms within the crystal lattice and allows researchers to characterize the material's structure. The observed variations in the (3 1 1) plane suggest that different concentrations of $FeCl_3$ impact the growth kinetics of the particles during synthesis, leading to variations in the final crystallite size. This phenomenon underscores the sensitivity of nanoparticle synthesis to the reaction conditions, emphasizing the need for precise control over parameters such as $FeCl_3$ concentration to achieve desired particle characteristics [35].

The MFSNC was designed to exhibit both magnetic and fluorescence properties. For the latter, the MFSNC samples were analyzed by a fluorescent spectrometer. Figure 3

Table 2 XRD parameters

Samples ID	FWHM	2θ(°)	d-spacing (A)	$D_{(311)}$(nm)
MFSNC0.5	0.33	35.597	2.52	26.3972
MFSNC1.0	0.65	35.609	2.5192	13.4021
MFSNC1.5	0.85	35.55	2.5232	10.2470
MFSNC2.0	0.73	35.567	2.5221	11.9320

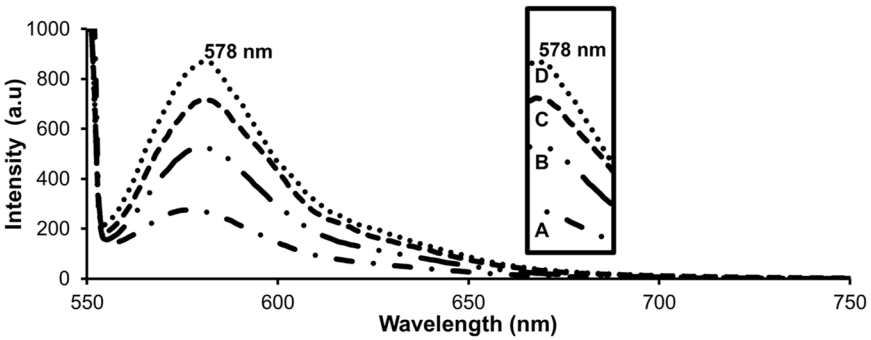

Fig. 3 Fluorescence spectra of MFSNC sample MFSNC0.5 (A), MFSNC1.5 (B), and MFSNC2.0 (C) and MFSNC1.0 (D) at an excitation wavelength of 545 nm

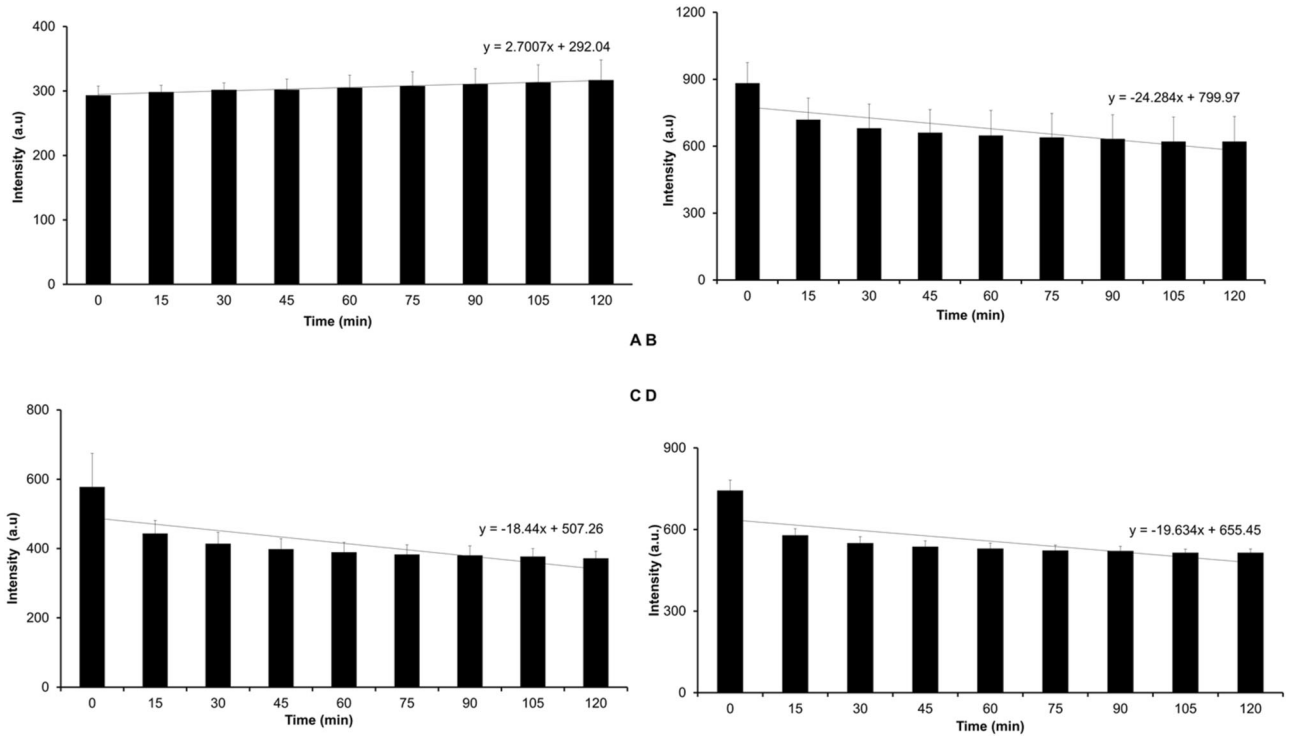

Fig. 4 Stability graph of MFSNC sample MFSNC0.5 (A), MFSNC1.0 (B), MFSNC1.5 (C), and MFSNC2.0 (D)

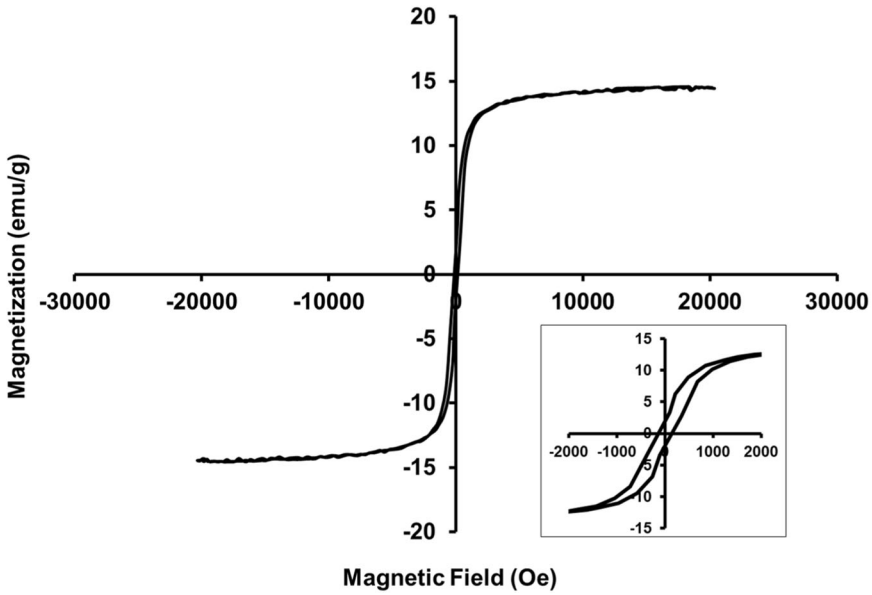

Fig. 5 Hysteresis loops of MFSNC

showed that the MFSNC could be examined for its fluorescence emission within the wavelength range of 550–750 nm, with an excitation wavelength of 545 nm. The maximum fluorescence intensity was observed at 578 nm, where MFSNC0.1 exhibited the greatest value of 852 a.u., whilst MFSNC0.5 had the lowest value of 280 a.u.

This study further investigates the fluorescence stability at the maximum emission wavelength of 578 nm for each sample variation over the interval of 120 min. Figure 4 illustrates that the MFSNC0.5 was more stable than other samples. The MFSNC0.1 sample had the maximum fluorescence intensity compared to the other samples. However, it demonstrated less photostability over time, with a

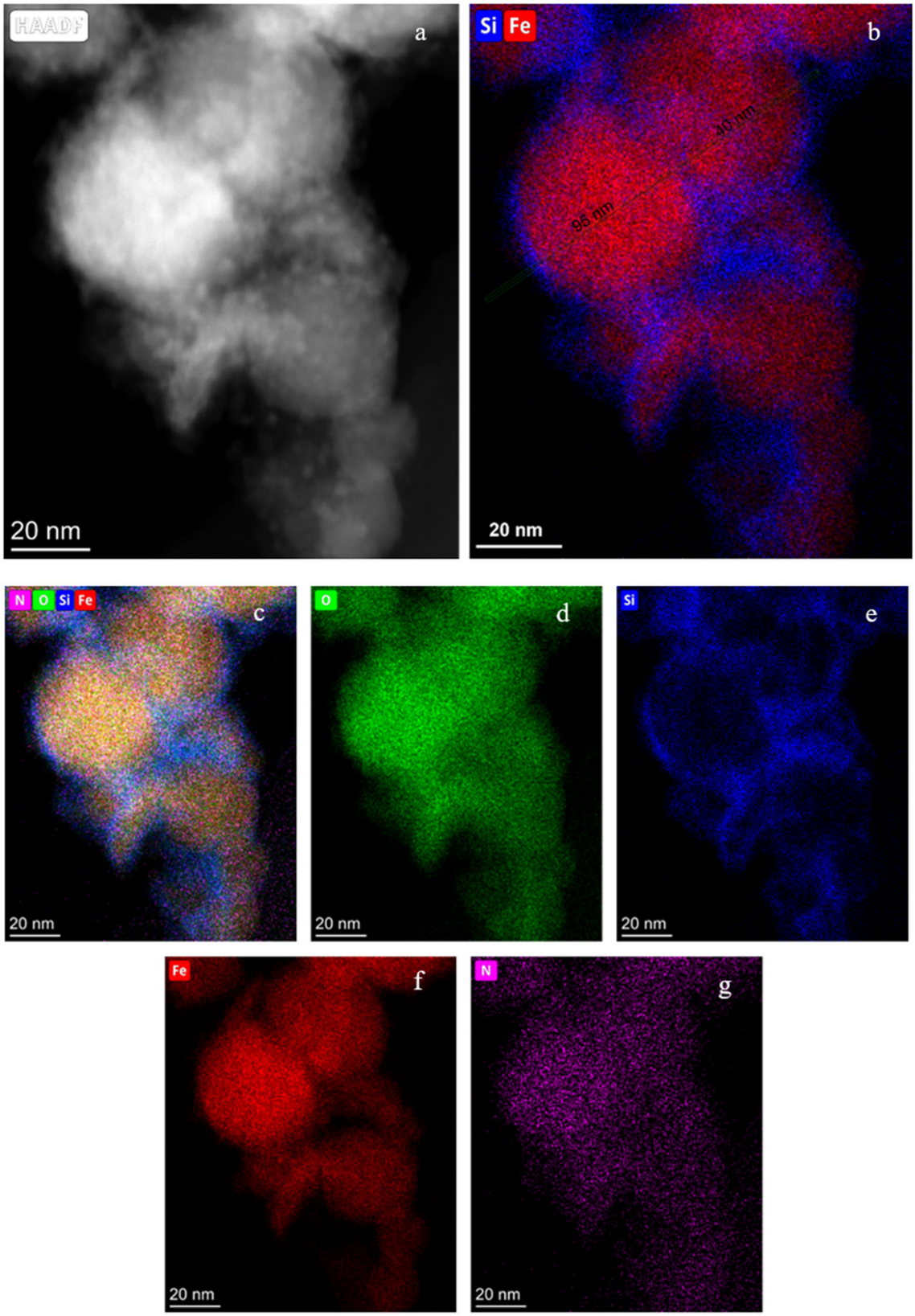

Fig. 6 TEM micrographs of the optimized MFSNC sample (**a**) and the corresponding EDX spectroscopy mapping: Si-Fe-K (**b**) N-O-Si-Fe-K (**c**) O-K (**d**) Si-K (**e**) Fe-K (**f**) and N-K (**g**), The incident electron beam was at 90 nA

Table 3 Comparison between different synthesis methods of silica-coated iron oxide with different precursors

Precursor	Methods	Type magnetization	Ms (emu/g)	Ref.
Iron-oxide and TEOS	Solvothermal method	Superparamagnetic	5.8	[34]
$FeCl_3.6H_2O$, EG, TEOS, QDs	A combination process of the solvothermal method, sol–gel method, and assembling method	Superparamagnetic	12.50	[41]
TEOS, Quercetin (QC), Fe_3O_4-PEG 3000 monodispere	Precipitated	Superparamagnetic	10.77	[42]
magnetite (Fe_3O_4), TEOS, and CdTe QDs	Precipitated	Superparamagnetic	11.18	[43]
$Y_{0.9}Ln_{0.1}VO_4$, Fe_3O_4, and TEOS	Stöber method	Superparamagnetic	14.39	[44]
Iron oxide nanoparticles and TEOS	Precipitated	Superparamagnetic	6.848	[45]
Iron Oxide, Silica Geothermal, and Rhodamin B	Sol–gel method	Ferromagnetic	14.57	This work

decrease in intensity of around 27% [36]. Considering the photostability of the sample, MFSNC0.5 was determined as the optimum sample.

The conventional magnetic hysteresis loop measurement provided an analysis of the magnetic properties of the optimized MFSNC sample, i.e., MFSNC0.5. The hysteresis loop is a magnetization curve representing a material of magnetic behavior of the multiple domains. It occurs because all the domains can not return to their original orientations after the magnetic saturation (Ms) is obtained and the field is decreased. There is remnant magnetization (MR) which can be removed by applying a magnetic field opposite the initially used field, defined as the coercive field (Hc). The mass magnetization at 300 °K was measured because it is assumed that the magnetic of materials is used near room temperature. At the same time, the magnetic response of the bare silica was minimal [9, 37]. Hence, Fig. 5 represented that the resulting MFSNC0.5 materials had a magnetization saturation of 14.57 emu/g and a loop area value of 0.7 kOe confirming the type of magnetization was ferromagnetic.

Ferromagnetism is the most intense magnetism, which has a spontaneous magnetic phenomenon and is produced by the self-alignment of the unpaired (same spin) forming electronic configurations of compounds (e.g., Fe, Co, Ni, Cr, Mn, and some rare earth). Ferromagnetic materials have magnetic properties highly dependent on anisotropy, including structure, shape, and surface anisotropy and generally recognized as either hard (permanent) magnets or soft magnets (i.e., rapidly/easily demagnetize) [38, 39]. It was reported that the iron oxide with coating agents will decrease magnetic saturation. The low magnetic saturation was presented by several phenomena relevant to the size of the synthesized particles, including finite size effect and change in cation distribution, shape effect or spin pinning, spin canting, crystal defect (amorphous), etc. [32]. The MFSNC sample had shown low coercivity arising from their soft-magnetic properties. In this study, the prepared MFSNC gave a relatively large diameter without superparamagnetic behavior, such as using temperature. Temperature influences the ferromagnetic, determined above a critical temperature value (i.e., Curie point, Tc) [38].

The FE-TEM images and its corresponding EDX mapping of the optimized MFSNC0.5 as shown in Fig. 6. The samples were clearly in their nanocomposite form with around 60 nm in diameter with the Fe_3O_4 size of around 40 nm (in red). The result further confirms the XRD crystallite results were the average size was calculated using the Scherrer equation as shown in Table 2 [11, 40].

Table 3 encapsulates a comprehensive exploration of diverse synthesis methods, magnetization types, and saturation magnetization (Ms) values for magnetic nanoparticles or nanocomposites derived from different precursors. The optimized MFSNC generated form this work was compared with previous studies and showed comparable magnetic properties to other nanomaterials derived from commercial precursors.

4 Conclusion

In conclusion, this study successfully synthesized MFSNC from natural geothermal silica, leading to materials that exhibit both magnetic and fluorescent characteristics. The XRD patterns, particularly the (3 1 1) peak, provided insights into the crystallite size variations influenced by different concentrations of ferric chloride during synthesis. The fluorescence spectra analysis highlighted the varying fluorescence intensities among MFSNC samples, with MFSNC0.5 showing the most stable fluorescence over time. The ferromagnetic behavior of MFSNC0.5, demonstrated by the hysteresis loop, indicated its suitability for applications requiring magnetic properties. The photostability graph further confirmed MFSNC0.5 as the optimized sample with dual magnetite and fluorescence properties. The TEM micrographs and EDX mapping provided a nanoscale

view of the MFSNC sample, reinforcing the findings from XRD and offering valuable insights into the material's microscopic structure and elemental distribution. Comparative analysis with other studies using different precursors and synthesis methods underscored the uniqueness of the synthesized MFSNC materials, particularly in exhibiting ferromagnetic properties. This research contributes valuable information on the synthesis and characterization of MFSNC materials, emphasizing their potential applications in diverse fields, such as biomedical imaging and sensing. The combination of magnetic and fluorescent properties opens up avenues for multifunctional applications, highlighting the importance of understanding how different synthesis parameters influence the properties of nanocomposites.

Acknowledgements The authors would like to acknowledge financial support from the JFS SEA-EU/ NAPARBA Project Grant no. SEA-EUROPE JFS19 ST-117 and the BRIN Riset & Inovasi untuk Indonesia Maju (RIIM) Grant No. 19/II.7/HK/2023. The authors acknowledge the facilities, scientific and technical support from the Advanced Characterization Laboratories of the National Research and Innovation Agency (BRIN) through E-Layanan Sains. SNAJ is the main contributor of this manuscript.

References

1. Jenie SNA, Kristiani A, Sudiyarmanto DS, Khaerudini K, dan Takeishi (2020) Sulfonated magnetic nanobiochar as heterogeneous acid catalyst for esterification reaction. J Environ Chem Eng 8:103912. https://doi.org/10.1016/j.jece.2020.103912
2. Lokhat D, Brijlal S, Naidoo DE, Premraj C, dan Kadwa E (2022) Synthesis of size-and-shape-controlled iron oxide nanoparticles via coprecipitation and in situ magnetic separation. Ind Eng Chem Res 61:16980–16991. https://doi.org/10.1021/acs.iecr.2c02350
3. Escoda-Torroella M, Moya C, Rodríguez AF, Batlle X, dan Labarta A (2021) Selective control over the morphology and the oxidation state of iron oxide nanoparticles. Langmuir 37:35–45. https://doi.org/10.1021/acs.langmuir.0c02221
4. Abdelaziz MM, Hefnawy A, Anter A, Abdellatif MM, Khalil MAF, dan Khalil IA (2022) Silica-coated magnetic nanoparticles for vancomycin conjugation. ACS Omega 7:30161–30170. https://doi.org/10.1021/acsomega.2c03226
5. Sanna Angotzi M, Mameli V, Zákutná D, Rusta N, dan Cannas C (2023) On the thermal and hydrothermal stability of spinel iron oxide nanoparticles as single and core-shell hard-soft phases. J Alloy Compd 940:168909. https://doi.org/10.1016/j.jallcom.2023.168909
6. Sodipo BK, dan Aziz AA (2016) Recent advances in synthesis and surface modification of superparamagnetic iron oxide nanoparticles with silica. J Magn Magn Mater 416:275–291. https://doi.org/10.1016/j.jmmm.2016.05.019
7. Sabale S, Khot V, Jadhav V, Zhu X, dan Xu Y (2014) Synthesis and properties of monodisperse superparamagnetic $Mg_{0.8}Mn_{0.2}Fe_2O_4$ nanoparticles using polyol reflux method. Acta Metall Sin Engl Lett 27:1122–1126. https://doi.org/10.1007/s40195-014-0139-y
8. Miguel MG, Lourenço JP, dan Faleiro ML (2020) Superparamagnetic iron oxide nanoparticles and essential oils: a new tool for biological applications. Int J Mol Sci 21:6633. https://doi.org/10.3390/ijms21186633
9. Kohaku K, Inoue M, Kanoh H, Taniguchi T, Kishikawa K, dan Kohri M (2020) Full-color magnetic nanoparticles based on holmium-doped polymers. ACS Appl Polym Mater 2:1800–1806. https://doi.org/10.1021/acsapm.0c00038
10. Han Q (2019) Controllable fabrication of magnetic core–shell nanocomposites with high peroxide mimetic properties for bacterial detection and antibacterial applications. J Mater Chem B 7:1124–1132. https://doi.org/10.1039/C8TB02834F
11. Khalid A, Ahmed RM, Taha M, dan Soliman TS (2023) Fe_3O_4 nanoparticles and Fe_3O_4 @SiO_2 core-shell: synthesize, structural, morphological, linear, and nonlinear optical properties. J Alloy Compd 947:169639. https://doi.org/10.1016/j.jallcom.2023.169639
12. Fatimah I (2022) Magnetic-silica nanocomposites and the functionalized forms for environment and medical applications: a review. Inorg Chem Commun 137:109213. https://doi.org/10.1016/j.inoche.2022.109213
13. Stolyar SV (2022) Manifestation of stoichiometry deviation in silica-coated magnetite nanoparticles. J Phys Chem C 126:7510–7516. https://doi.org/10.1021/acs.jpcc.2c00349
14. Ghosh A, Srinivas V, Kavita S, dan Sundara R (2022) Evolution of microstructure and magnetic properties from amorphous Fe_3O_4/SiO_2 nanocomposite. J Magn Magn Mater 561:169687. https://doi.org/10.1016/j.jmmm.2022.169687
15. Ali Z, Andreassen J-P, dan Bandyopadhyay S (2023) Fine-tuning of particle size and morphology of silica coated iron oxide nanoparticles. Ind Eng Chem Res 62:4831–4839. https://doi.org/10.1021/acs.iecr.2c03338
16. Souza KC, Mohallem NDS, dan Sousa EMB (2010) Mesoporous silica-magnetite nanocomposite: facile synthesis route for application in hyperthermia. J Sol Gel Sci Technol 53:418–427. https://doi.org/10.1007/s10971-009-2115-y
17. Sabale S, Jadhav V, Mane-Gavade S, dan Yu X-Y (2019) Superparamagnetic CoFe2O4@Au with high specific absorption rate and intrinsic loss power for magnetic fluid hyperthermia applications. Acta Metall Sin Engl Lett 32:719–725. https://doi.org/10.1007/s40195-018-0830-5
18. Elmaria FA, dan Jenie SNA (2021) Magnetic nanoparticles based on natural silica as a methyl ester forming acid catalyst. J Kim Terap Indones 23:49–54. https://doi.org/10.14203/inajac.v23i2.473
19. DA Widyasari, Conjugation of E. coli antibody with fluorescent natural silica-based nanoparticles: preparation and characterization, dipresentasikan pada. In Proceedings of the 4th international seminar on metallurgy and materials (ISMM2020): accelerating research and innovation on metallurgy and materials for inclusive and sustainable industry, Tangerang Selatan, Indonesia, 2021, 030009. https://doi.org/10.1063/5.0060386.
20. V Gubala, G Giovannini, F Kunc, MP Monopoli, CJ dan Moore Dye-doped silica nanoparticles: synthesis, surface chemistry and bioapplications. *Cancer Nanotechnol* 11 2020. https://doi.org/10.1186/s12645-019-0056-x.
21. He H, Sun D-W, Wu Z, Pu H, dan Wei Q (2022) On-off-on fluorescent nanosensing: Materials, detection strategies and recent food applications. Trends Food Sci Technol 119:243–256. https://doi.org/10.1016/j.tifs.2021.11.029
22. Rong H, Gao T, dan Zhang X (2020) Improved fluorescence stability for Fe3O4/silica @fluorescein/dense silica structure with double shell. Compos Commun 20:100368. https://doi.org/10.1016/j.coco.2020.100368
23. Jenie ASN (2020) Geothermal silica-based fluorescent nanoparticles for the visualization of latent fingerprints. Mater Express 10:258–266. https://doi.org/10.1166/mex.2020.1551

24. Sifana NO, dan Jenie SNA (2022) Fabrication and characterization of FITC-modified naturalbased silica nanoparticles using sol-gel method. IOP Conf Ser Earth Environ Sci 963:012025. https://doi.org/10.1088/1755-1315/963/1/012025
25. Silviana S (2022) Superhydrophobic coating based on silica derived from bagasse modified with vinyltriethoxysilane and copper (Cu) as antibacterial agent. IOP Conf Ser Earth Environ Sci 963:012023. https://doi.org/10.1088/1755-1315/963/1/012023
26. Selvaraj R (2022) A recent update on green synthesized iron and iron oxide nanoparticles for environmental applications. Chemosphere 308:136331. https://doi.org/10.1016/j.chemosphere.2022.136331
27. Polla MB (2023) Low-temperature sol–gel synthesis of magnetite superparamagnetic nanoparticles: Influence of heat treatment and citrate–nitrate equivalence ratio. Ceram Int 49:7322–7332. https://doi.org/10.1016/j.ceramint.2022.10.182
28. Sharma RK (2023) Influence of chemical and bio-surfactants on physiochemical properties in mesoporous silica nanoparticles synthesis. J Mater Res Technol 24:2629–2639. https://doi.org/10.1016/j.jmrt.2023.03.170
29. Jenie SNA (2021) Rapid fluorescence quenching detection of Escherichia coli using natural silica-based nanoparticles. Sensors 21:881. https://doi.org/10.3390/s21030881
30. Syakina AN, dan Rahmayanti M (2023) Removal of methyl violet from aqueous solutions by green synthesized magnetite nanoparticles with Parkia Speciosa Hassk. peel extracts. Chem Data Collect 44:101003. https://doi.org/10.1016/j.cdc.2023.101003
31. Feng T (2023) Engineering Ru nanoparticles embedded in 2D N-doped carbon nanosheets decorated with 2D Fe_3O_4–Fe_3C heterostructures for efficient hydrogen evolution in alkaline and acidic media. Int J Hydrog Energy 48:15522–15532. https://doi.org/10.1016/j.ijhydene.2023.01.022
32. Kornilitsina EV (2023) Enhanced electrodynamic properties acrylonitrile butadiene styrene composites containing short-chopped recycled carbon fibers and magnetite. Diam Relat Mater 135:109814. https://doi.org/10.1016/j.diamond.2023.109814
33. Tian Y (2021) Aptamer modified magnetic nanoparticles coupled with fluorescent quantum dots for efficient separation and detection of Alicyclobacillus acidoterrestris in fruit juices. Food Control 126:108060. https://doi.org/10.1016/j.foodcont.2021.108060
34. Wu X, dan Nan Z (2019) Degradation of rhodamine B by a novel Fe_3O_4/SiO_2 double-mesoporous-shelled hollow spheres through photo-Fenton process. Mater Chem Phys 227:302–312. https://doi.org/10.1016/j.matchemphys.2019.02.023
35. Koesnarpadi S, Santosa SJ, Siswanta D, dan Rusdiarso B (2017) Humic acid coated Fe_3O_4 nanoparticle for phenol sorption. Indones J Chem 17:274. https://doi.org/10.22146/ijc.22545
36. Yang L (2021) Fluorescent core-shell SiO2@vertical covalent organic frameworks nanosheets for sensing application. Sens Actuators B Chem 341:129995. https://doi.org/10.1016/j.snb.2021.129995
37. Sandler SE, Fellows B, dan Mefford OT (2019) Best practices for characterization of magnetic nanoparticles for biomedical applications. Anal Chem 91:14159–14169. https://doi.org/10.1021/acs.analchem.9b03518
38. Nisticò R (2021) A synthetic guide toward the tailored production of magnetic iron oxide nanoparticles. Bol Soc Esp Cerám Vidr 60:29–40. https://doi.org/10.1016/j.bsecv.2020.01.011
39. Ma Z, Mohapatra J, Wei K, Liu JP, dan Sun S (2023) Magnetic nanoparticles: synthesis, anisotropy, and applications. Chem Rev 123:3904–3943. https://doi.org/10.1021/acs.chemrev.1c00860
40. Aliya S (2023) Phytogenic fabrication of iron oxide nanoparticles and evaluation of their in vitro antibacterial and cytotoxic activity. Arab J Chem 16:104703. https://doi.org/10.1016/j.arabjc.2023.104703
41. Huang Z (2019) A novel method based on fluorescent magnetic nanobeads for rapid detection of Escherichia coli O157:H7. Food Chem 276:333–341. https://doi.org/10.1016/j.foodchem.2018.09.164
42. Halevas E (2020) Modified magnetic core-shell mesoporous silica nano-formulations with encapsulated quercetin exhibit anti-amyloid and antioxidant activity. J Inorg Biochem 213:111271. https://doi.org/10.1016/j.jinorgbio.2020.111271
43. Wang M, dan Deng M (2022) Synthesis and characterization of fluorescent magnetic Fe_3O_4/CdTe@SiO_2-NH-FA nanoprobe. Mater Lett 309:131358. https://doi.org/10.1016/j.matlet.2021.131358
44. Lacerda Fernandes Í (2022) Synthesis and characterization of the MNP@SiO_2@TiO_2 nanocomposite showing strong photocatalytic activity against methylene blue dye. Appl Surf Sci 580:152195. https://doi.org/10.1016/j.apsusc.2021.152195
45. Fahmy HM, Saad OA, dan Fathy MM (2023) Insight into the photothermal therapeutic impacts of silica-coated iron oxide nanocomposites. J Drug Deliv Sci Technol 84:104540. https://doi.org/10.1016/j.jddst.2023.104540